



# Synergistic effect in plasmonic Au/Ag alloy NPs co-coated TiO<sub>2</sub> NWs toward visible-light enhanced CO<sub>2</sub> photoreduction to fuels



Muhammad Tahir\*, Beenish Tahir, Nor Aishah Saidina Amin

Chemical Reaction Engineering Group, Department of Chemical Engineering, Faculty of Chemical and Energy Engineering, Universiti Teknologi Malaysia, 81310, UTM, Skudai, Johor Baharu, Johor, Malaysia

## ARTICLE INFO

### Article history:

Received 29 June 2016

Received in revised form

25 November 2016

Accepted 30 November 2016

Available online 5 December 2016

### Keywords:

Plasmonic Au-Ag alloy

TiO<sub>2</sub> NWs

Synergistic effect

CO<sub>2</sub> photoreduction

H<sub>2</sub> reductant

Visible light

## ABSTRACT

Plasmonic Au/Ag alloy NPs supported on TiO<sub>2</sub> nanowires (TiO<sub>2</sub> NWs) have been designed and synthesized through a facile hydrothermal and photo-deposition method. The samples were characterized by XRD, FE-SEM, TEM, N<sub>2</sub>-adsorption-desorption, XPS, Raman, UV-vis and PL spectroscopy. Bimetallic Au/Ag NPs were presented over the TiO<sub>2</sub> NWs as an alloy, thus exhibited strong absorption of visible light due to the localized surface plasmon resonance (LSPR) excitation. The synergistic effect in plasmonic Au/Ag alloy NPs for selective photocatalytic CO<sub>2</sub> reduction with H<sub>2</sub> to CO and hydrocarbons under visible light irradiation was investigated. The present design of plasmonic Au/Ag NPs co-decorated TiO<sub>2</sub> NWs leads to remarkably enhanced photoactivity of CO<sub>2</sub> reduction to CO. The CO evolution rate as a main product over the Au-Ag alloy NPs coated TiO<sub>2</sub> NWs was 1813 μmole-g-catal.<sup>-1</sup> h<sup>-1</sup> at selectivity 98%. This amount was approximately 1.72 time larger comparing to Au-NPs/TiO<sub>2</sub> NWs, 1.84 fold more than the Ag-NPs/TiO<sub>2</sub> NWs, 72.52 fold than the TiO<sub>2</sub> NWs and 201 fold more than the amount of CO produced over the bare TiO<sub>2</sub>-NPs. This great enhancement can be attributed to synergistic effects in Au/Ag-NPs, enhanced visible light absorption due to Au-Ag alloy formation and improved charge separation in LSPR-excited TiO<sub>2</sub> NWs. In addition, turnover productivity is introduced to investigate the effect of operating parameters on the performance of photocatalysts. The plasmonic reaction mechanism of Au-Ag NPs in conjunction with LSPR excitation and charge transport to understand the reaction pathway is described.

© 2016 Elsevier B.V. All rights reserved.

## 1. Introduction

Transformation of CO<sub>2</sub> to more value added chemicals is a promising carbon management approach to offset the cost of implementing CO<sub>2</sub> capturing technologies. Among the other alternatives, solar photocatalytic conversion of CO<sub>2</sub> appears the most prospective path, since it would be helpful to lessen atmospheric CO<sub>2</sub> level and can partly achieve energy demands [1–3]. The most of the work in photocatalytic CO<sub>2</sub> reduction has been related to using water as a reducing agent. Generally, the main products during the photo-induced CO<sub>2</sub> and H<sub>2</sub>O reactions are CO and CH<sub>4</sub> using the gas phase photoreactor system [4–6], but the formation of CH<sub>3</sub>OH has also been reported [7]. However, H<sub>2</sub>O is hardly reducible and yielded lower CO<sub>2</sub> conversion efficiency and products selectivity [8]. Recently, reduction of CO<sub>2</sub> by H<sub>2</sub> to CO via photocat-

alytic reverse water gas shift (PRWGS) reaction has been the most attractive approach in CO<sub>2</sub> conversion applications [9,10].

Since the discovery of photocatalytic CO<sub>2</sub> reduction over the semiconductor materials, TiO<sub>2</sub> is one of the most widely used and promising photocatalyst because of its high activity, low-cost, non-toxicity, abundantly availability and chemically inertness [11,12]. However, the efficiency of the pure TiO<sub>2</sub> is low owing to fast recombination of photo-generated charges [13]. Besides, TiO<sub>2</sub> is functional only under ultraviolet (UV) light because of wide band gap energy (3.20 eV for anatase phase and ~3.0 eV for rutile phase). Recently, TiO<sub>2</sub> nanomaterials such as nanosheets, nanowires, nanorods and nanotubes are considered as the superior candidates in photocatalysis applications. These materials have distinctive physical and optical properties, thus offer a direct pathway for efficiently collecting photons and/or electrons. The one dimensional (1D) nanomaterials with regular structure can provide large surface area, thus enriched photo-generated charges transport and have hindered charges recombination rate [14–16]. Therefore, development of a photocatalytic system based on structured TiO<sub>2</sub> that could utilize solar energy is important for practical applications.

\* Corresponding author. Permanent address: Department of Chemical Engineering, COMSATS Institute of Information Technology Lahore, Punjab, Pakistan.

E-mail addresses: [mtahir@cheme.utm.my](mailto:mtahir@cheme.utm.my), [bttahir@yahoo.com](mailto:bttahir@yahoo.com) (M. Tahir).

Many approaches to develop solar active  $\text{TiO}_2$  nanomaterials including doping and photosensitization have been suggested by many researchers. Metal-doping is one the most favorable approach for narrowing the band gap energy, while metal-doped ions in  $\text{TiO}_2$  act as a barrier and prevented photo-excited electrons and holes recombination. Noble metal nanoparticles such as gold nanoparticles (Au-NPs) and silver nanoparticles (Ag-NPs) have been successfully reported as photosensitizers to improve  $\text{TiO}_2$  photocatalytic efficiency under visible light [17,18]. These metals have strong absorption of visible light based on their characteristics of localized surface plasmon resonance (LSPR). In LSPR-excitation, light energy can be coupled into metal NPs and plasmon-induced electrons can be injected to semiconductor to make it visible light active [19]. Moreover, noble metal NPs possess electron storage properties, resulting in improved electron-hole pair separation in metal-semiconductor composite system [20].

During the last years, a number of reports relating to photocatalytic activity of LSPR induced  $\text{TiO}_2$  and its mechanism under visible light irradiation has been presented [21–24]. LSPR induced  $\text{TiO}_2$  by Au-NPs have been reported by many researchers [25–28]. The photo-deposited Au-NPs onto  $\text{TiO}_2$  for  $\text{CO}_2$  reduction to hydrocarbons have proven significant effect on the photocatalytic activity and products selectivity [29]. Photocatalytic  $\text{CO}_2$  reduction to  $\text{CH}_4$  over macro-porous  $\text{TiO}_2$ -supported Au-NPs has been reported with improved photoactivity due Au-NPs LSPR effects [30]. When, Au/Pt NPs decorated  $\text{TiO}_2$  nanofibers were used for photocatalytic  $\text{H}_2$  production and  $\text{CO}_2$  reduction, Au-NPs facilitated for visible light absorption trough the LSPR effect, while Pt served as an electrons sink to retard the charges recombination rate [22]. Recently, we investigated Au-NPs-promoted  $\text{TiO}_2$  nanowires for selective photocatalytic  $\text{CO}_2$  reduction to CO. Significantly improved  $\text{TiO}_2$  activity under visible light was observed by LSPR effect of Au-NPs [31]. On the other hand, Ag-NPs have been also proven to give strong visible light absorption based on the LSPR [32,33]. Liu et al. [34] reported photocatalytic  $\text{CO}_2$  reduction with  $\text{H}_2\text{O}$  to  $\text{CH}_3\text{OH}$  over plasmonic Ag/ $\text{TiO}_2$  NWs under visible light. The improved  $\text{TiO}_2$  photoactivity for  $\text{CH}_3\text{OH}$  production was observed due to Ag-NPs LSPR effect.

So far most of the previously reported Au and Ag based  $\text{TiO}_2$  composites have been prepared using spherical  $\text{TiO}_2$  nanoparticles with single metal loading. Only limited reports demonstrate LSPR driven  $\text{CO}_2$  reduction over plasmon-induced  $\text{TiO}_2$  under visible light. Au/Ag NPs loaded rutile  $\text{TiO}_2$  photocatalyst has been investigated for photo-decomposition of 2-propanol. The photocatalytic activity was significantly enhanced due to electron injection from LSPR excited Au/Ag NPs into  $\text{TiO}_2$  under visible light [35]. Recently, the synergistic effect in Ag-In electro-catalysts for  $\text{CO}_2$  reduction has been demonstrated with enhanced photoactivity and selectivity [36]. Furthermore, the wavelength tuning of LSPR system can be achieved by modifying the size, shape and type of noble metals loaded over the  $\text{TiO}_2$  surface. In this perspective, a promising approach is the use of Au-Ag alloy, which can absorb visible light over a broad range of solar spectrum. Verbruggen et al. [37] synthesized Au-Ag alloy NPs supported on the  $\text{TiO}_2$  and reported tunable visible light activity toward the degradation of stearic acid. Therefore, it is of great importance to explore synergistic effects in Au/Ag bimetallic nanoparticles supported on the  $\text{TiO}_2$  NWs for visible light applications. The present research aimed to investigate synergistic effect in Au/Ag alloy NPs decorated on  $\text{TiO}_2$  NWs for LSPR-induced  $\text{CO}_2$  reaction by  $\text{H}_2$  to provide a way to absorb visible light and could improve photoactivity for selective solar fuels.

Herein, we designed and synthesized Au-Ag bimetallic nanoparticles supported on  $\text{TiO}_2$  NWs and discussed their synergistic effects for LSPR-excitation under visible light. Au-NPs loaded  $\text{TiO}_2$  NWs were synthesized by a modified hydrothermal and a chemical reduction route, while the Ag-NPs were photo-deposited onto  $\text{TiO}_2$  NWs. Au-Ag alloy was synthesized by a chemical reduction and

photo-deposition under UVA illumination. The structured nanocatalysts were investigated for plasmon-induced  $\text{CO}_2$  reduction to CO and hydrocarbons using  $\text{H}_2$  as a reductant. More importantly, the turn over productivity (TOP) analysis is introduced for systematic understanding the effect of operating parameters on the activity of photocatalysts. The photocatalytic reaction process in conjunction with LSPR is critically discussed to understand the synergistic effect in Au-Ag NPs toward  $\text{CO}_2$  reduction.

## 2. Experimental

### 2.1. Synthesis of $\text{TiO}_2$ NWs

Initially,  $\text{TiO}_2$  nanoparticles were synthesized through a simple and direct sol-gel method according to our previous work [4].  $\text{TiO}_2$  NWs were prepared using a facile hydrothermal synthesis technique as follows (refer to Fig. 1). First, 1 g  $\text{TiO}_2$  NPs was suspended in 8 M NaOH solution (50 mL) and stirred for 10 min. The sample was then transferred into Teflon-lined continuous stirred reactor and heated to 110 °C under continuous stirring for 2 h before the mixture was cooled to room temperature. The obtained suspension of  $\text{TiO}_2$  NWs was washed with deionized to get pH below 9. Finally, crystals were washed with 0.1 M HCl and deionized water to ensure no residual ions left in the sample. After being dried at 80 °C for 12 h, the samples were calcined at 500 °C for 5 h before stored in airtight glass bottles.

### 2.2. Preparation of Au/Ag NPs loaded $\text{TiO}_2$ NWs

The deposition of gold and silver nanoparticles on the  $\text{TiO}_2$  NWs was conducted with a chemical reduction and photo-deposition method. Au-NPs coated  $\text{TiO}_2$  NWs were prepared by the procedure briefly described as follows (refer to Fig. 1). 0.50 g of  $\text{TiO}_2$  NWs powder was dispersed in 50 mL of ethylene glycol and the mixture was heated to 160 °C in a continuous stirred tank reactor. A certain volume of 0.025 M  $\text{AuCl}_2$  solution was injected rapidly into solution and stirred for 10 min at 160 °C before the mixture was cooled to room temperature. The solids were filtered and oven dried at 80 °C for 12 h. The different volumes of  $\text{AuCl}_2$  solution were used to get Au loading of 0.1%, 0.3%, 0.5% and 0.7 wt.%, respectively. Similar procedure was used to prepare Ag-NPs supported over  $\text{TiO}_2$  NWs. The different volumes of  $\text{AgNO}_3$  solution were used to get Ag loading of 2, 3, 5 and 7 wt.%, respectively. Finally, solids of Au and Ag loaded  $\text{TiO}_2$  NWs were calcined at 500 °C for 5 h under air flow.

### 2.3. Preparation of Au-Ag bimetallic nanoparticles supported $\text{TiO}_2$ NWs

The Au-Ag-NPs supported  $\text{TiO}_2$  NWs were prepared through a chemical and photoreduction method. Briefly, 0.5 wt.% Au-NPs-loaded  $\text{TiO}_2$  NWs were immersed in a certain volume of 0.025 M  $\text{AgNO}_3$  solution under continuous stirring. The mixture was then irradiated under UV-light irradiation using 200 W Hg lamp of light intensity 150 mW cm<sup>-2</sup> at wavelength 252 nm for 10 min to get gray precipitations before being dried in an oven at 80 °C for 12 h. Finally, the samples were calcined at 500 °C for 5 h to get final Au/Ag co-loaded  $\text{TiO}_2$  NWs. The different volumes of  $\text{AgNO}_3$  solution were used to get Ag loading of 1, 2, 3 and 5 wt.%, respectively. The schematics for the fabrication of Au/Ag-NPs loaded  $\text{TiO}_2$  NWs is depicted in Fig. 1.

### 2.4. Structure characterization

X-ray powder diffraction (XRD) was recorded on a Bruker D 8 advance diffractometer with Cu- K $\alpha$  radiation ( $\lambda=1.54\text{ \AA}^0$ , operated at 40 kV and 40 mA) to identify the phase structure and

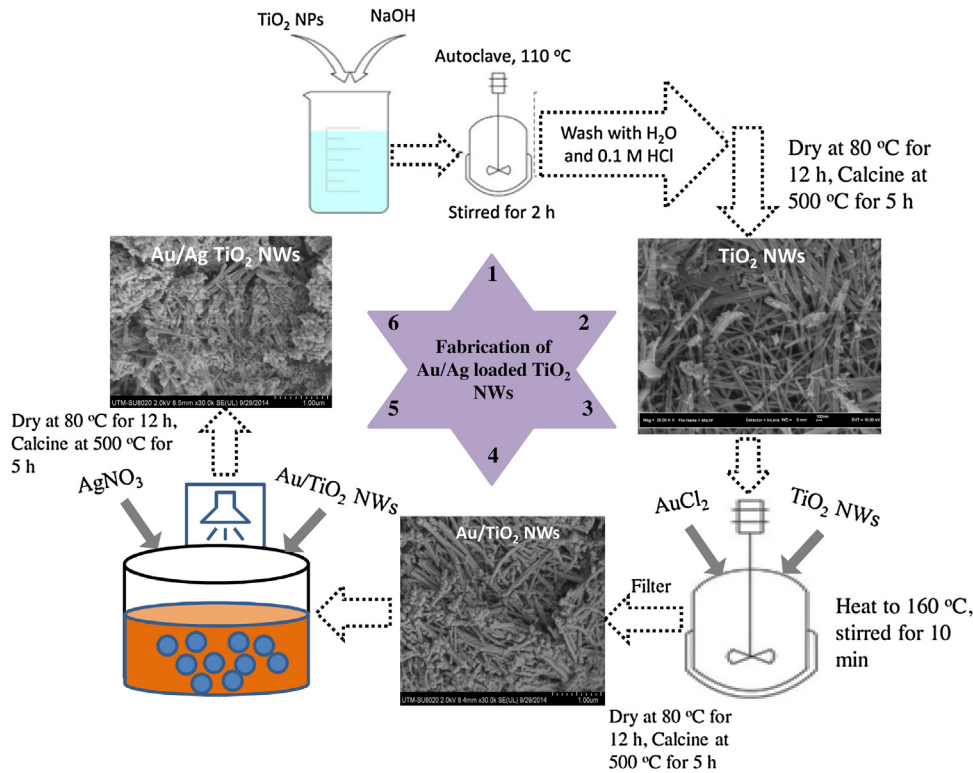


**Fig. 1.** Schematics for synthesis procedure of Au/Ag-NPs loaded TiO<sub>2</sub> nanowires.

phase transformation of all the samples. The morphology of the products was investigated using field-emission scanning electron microscopy (FE-SEM) with Carl Zeiss Supra 35 VP FE-SEM instrument. The transmission electron microscopy (TEM) was performed using JEOL-TEM apparatus operating with an acceleration voltage of 200 kV, which was used to measure the particle sizes and d-spacing of the samples. The XPS spectra were calibrated with respect to the binding energy of the C1s signal at 284.60 eV as an internal standard. Nitrogen-adsorption-desorption isotherms were collected using Micromeritics ASAP 2020 at 77 K. The samples were degassed at 523 K for 4 h under vacuum and by using the nitrogen flux. The Brunauer-Emmett-Teller (BET) surface area and pore diameters were calculated from the desorption branch of isotherms according to BJH method. Ultraviolet-visible (UV-vis) diffuse reflectance absorbance spectra were carried out on a Cary 100 Agilent UV-vis spectrophotometer equipped with an integrated sphere in the wavelength range of 200–800 nm. Raman and photoluminescence (PL) spectra of samples were recorded on a Raman Xplora Plus Spectrophotometer (HORIBA Scientific) with a 600 nm grating and a 532 nm emitting laser as an excitation source.

## 2.5. Photocatalytic testing and analysis

The photocatalytic CO<sub>2</sub> reduction with H<sub>2</sub> was carried out in a stainless steel rectangular reactor of total volume 108 cm<sup>3</sup> [4]. A 35W HID Xe lamp was used as a visible light source with a light intensity of 20 mW cm<sup>-2</sup> measured using a reference solar cell (91150 V, Newport). Similarly, a 200W Hg reflector lamp with a maximum light intensity of 150 mW cm<sup>-2</sup> was used as a source of UV-light irradiation. The UV-light intensity was measured using an online optical process monitor ILT OPM-1D and a SED008/W sensor. The lamps were located at the top of the reactor equipped with a quartz window of 10 mm thickness for the passing of light irradiations. Typically, powder photo-catalyst (10 mg) was evenly dispersed inside the bottom surface of the reactor. Compressed CO<sub>2</sub>

and H<sub>2</sub> (purity > 99.99%) regulated by mass flow controllers (MFC) were passed continuously through the reactor. The reactor pressure was maintained at 0.20 bars above the atmospheric pressure for the batch mode experiment by closing the outlet valves. The gas feed ratio of CO<sub>2</sub> and H<sub>2</sub> of 1 was used for all the experiments. The gaseous products were analyzed using an online gas chromatograph (GC-Agilent Technologies 6890 N, USA) equipped with FID and TCD detectors (GC/FID/TCD). The FID detector was connected with HP PLOT Q column while the TCD detector consisted of HP Plot Q, Porapak Q, DC-200, UCW-982 and MS 13X columns.

The quantum yield (QY) was calculated to compare the performance of photocatalytic system with the previous researchers work. If one photon is used to generate one electron-hole pair, then the reaction quantum yield (QY) for CO<sub>2</sub> photoreduction is defined as the ratio of photons converted into electrons to produce specific product (mole per sec) to the total photonic flux (mole per sec) entering into the reactor as illustrated in Eq. (1) [38].

$$\text{Quantum Yield (QY, %)} = \frac{n \times \text{moles of production rate (mol/sec)}}{\text{moles of photon flux (mol/sec)}} \times 100 \quad (1)$$

Where, n is the number of electrons required for the production of any specific product. In the specific case, 2, 6 and 8 electrons are needed for the production of CO, CH<sub>3</sub>OH and CH<sub>4</sub>. The moles of photon could be calculated from the visible-light input energy of intensity 20 mW cm<sup>-2</sup>. Although, QY is an effective way to find photocatalytic system performance, yet this method is applicable at room temperature and atmospheric pressure and preferably used for slurry systems. In the case of gas phase system and in order to investigate the effects of process parameters such as catalyst loading, reactor volume, reactor pressure and temperature, the QY equation needed to be amended. Therefore, in this study, turn over productivity (TOP) is introduced to calculate the performance of the gas phase photocatalytic system as illustrated in Eq. (2).

$$\text{TOP (\%)} = \text{QY} \times \frac{PV}{nRT} \quad (2)$$

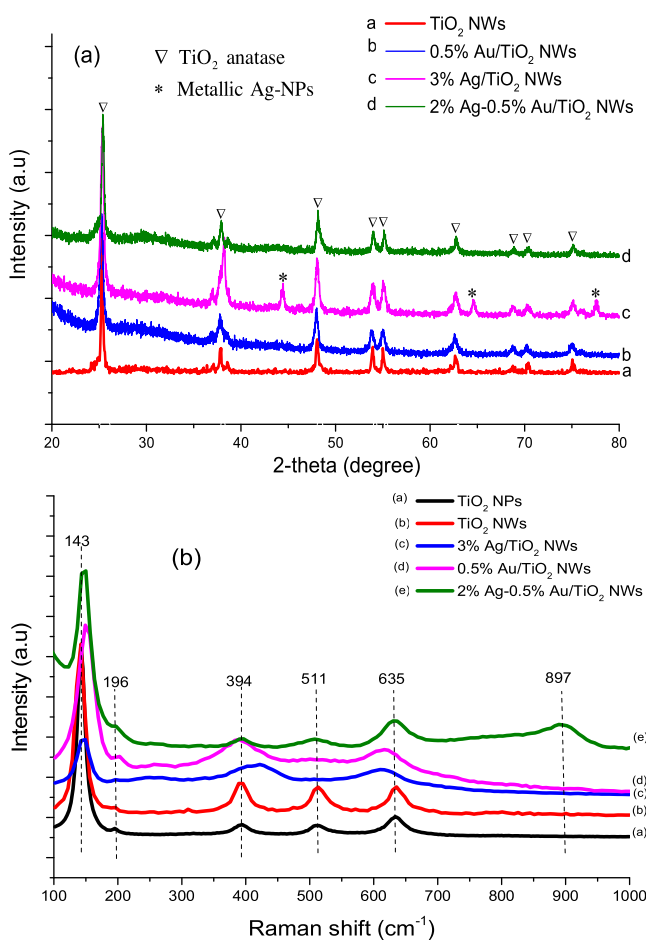


**Fig. 2.** (a) XRD patterns of different TiO<sub>2</sub> NWs loaded with Au/Ag nanoparticles; (b) Raman spectroscopy of TiO<sub>2</sub> NWs and Au/Ag loaded TiO<sub>2</sub> NWs.

Where,  $P$  is total reactor pressure,  $V$  is the reactor volume,  $n$  is moles of the catalyst used,  $T$  is the reaction temperature and  $R$  is the universal gas constant.

### 3. Results and discussion

#### 3.1. Characterization analysis of nano-materials

All the prepared TiO<sub>2</sub> NWs and Au/Ag NPs loaded TiO<sub>2</sub> NWs were characterized by X-ray diffraction (XRD) and Raman to investigate the phase purity and crystallinity as shown in Fig. 2. The XRD patterns of the pure TiO<sub>2</sub> NWs and Au/Ag-NPs loaded TiO<sub>2</sub> NWs calcined at 500 °C for 5 h are shown in Fig. 2(a). The TiO<sub>2</sub> NWs and Au/Ag-NPs loaded TiO<sub>2</sub> NWs were in the pure anatase and crystalline phase of TiO<sub>2</sub>. After modifying by Au/Ag nanoparticles, the diffraction peaks of TiO<sub>2</sub> NWs were unaltered. The spectrum of TiO<sub>2</sub> NWs with and without Au/Ag-NPs exhibits 2θ peaks located at 25.31°, 37.80°, 48.0°, 53.87°, 55.08°, 62.73°, 68.75°, 70.25° and 75.09°. All these peaks were consistent with (101), (004), (200), (105), (211), (204), (116), (220) and (215). This illustrates the presence of TiO<sub>2</sub> in anatase phase with growth axis in (101) directions when compared with JCPDS-ICSD standards for anatase (File No. 89-4921). However, Au-NPs peaks in Au-NPs/TiO<sub>2</sub> NWs were not detected to give any indication of the presence due to lower Au-contents.

On the other hand, the Ag-NPs peaks in the XRD pattern of Ag-NPs/TiO<sub>2</sub> NWs were detected at  $2\theta = 44.35^\circ$ ,  $64.65^\circ$  and  $77.62^\circ$ , consistent with (200), (220) and (311). This observation matches

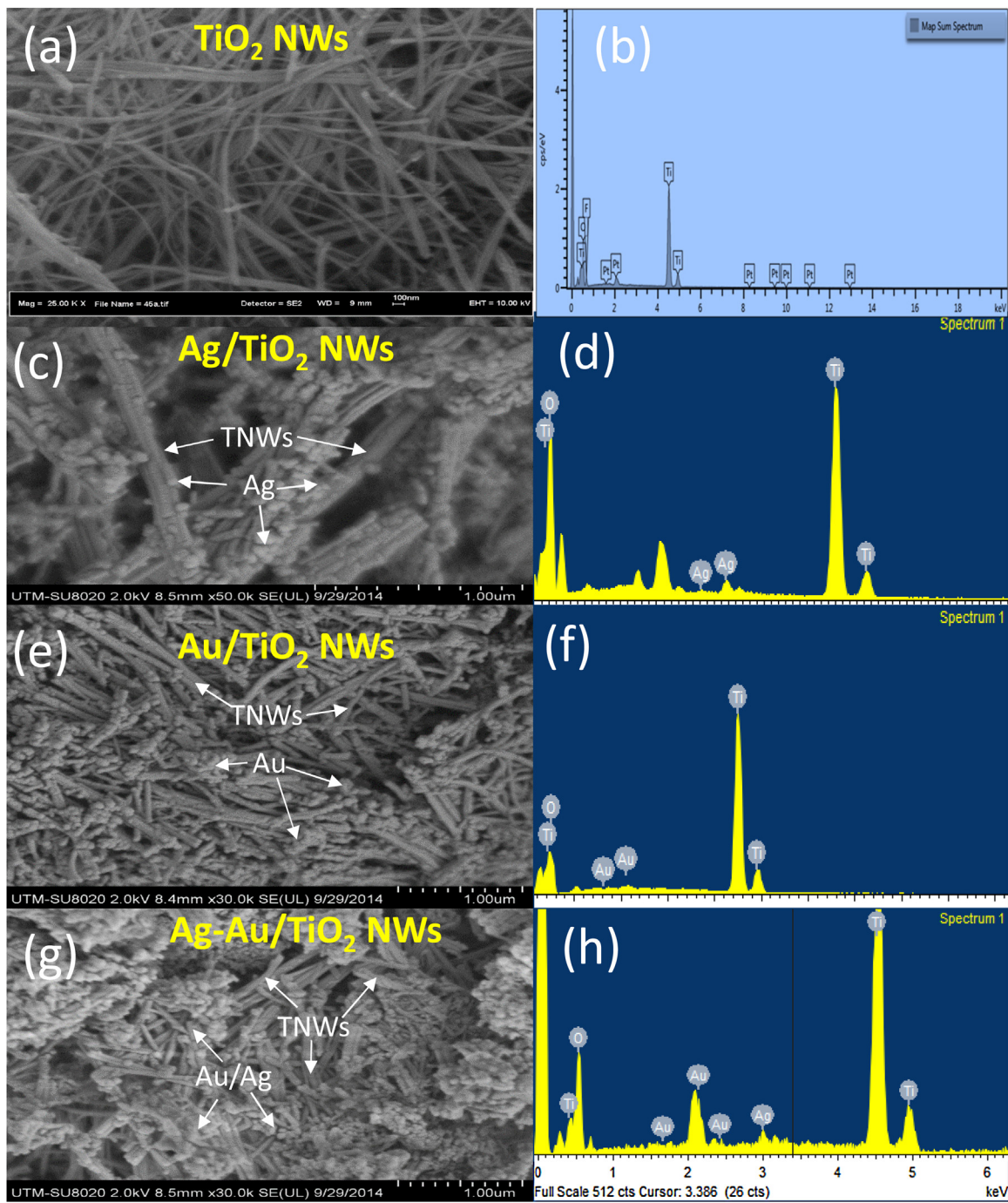
with JCPDS File No. 04-0783 and reflects metallic structure of the silver nanoparticles. More prominently, the peaks of Au/Ag NPs coated over the TiO<sub>2</sub> NWs were not detected, suggesting that Au and Ag species were combined together due to the formation of Au-Ag alloy and were probably due to the lower metal contents. Numerous reports have discussed the incorporation of metals and similar observations have been reported [39].

Fig. 2(b) presents the Raman spectrum of the pure TiO<sub>2</sub>, TiO<sub>2</sub> NWs and Au/Ag modified TiO<sub>2</sub> NWs samples. The observed peaks in the Raman spectrum of the TiO<sub>2</sub> samples are relatively sharp and stronger than the Au/Ag NPs loaded TiO<sub>2</sub> NWs samples. In the case of pure TiO<sub>2</sub> samples, the intense Raman signals with  $E_{g(1)}$  mode appeared at 143 cm<sup>-1</sup> followed by low intense modes  $E_{g(2)}$  and  $E_{g(3)}$  located at 196 cm<sup>-1</sup> and 635 cm<sup>-1</sup>, respectively.  $B_{1g}$  peak appeared at 394 cm<sup>-1</sup> and ( $A_{1g}$  +  $B_{1g}$ ) reflected as a single merged peak at 511 cm<sup>-1</sup>. All these peaks reveal the characteristics of the pure anatase phase of TiO<sub>2</sub>. The Raman vibrational modes are evidently due to the bending vibration of Ti—O—Ti bond. However, the intense  $E_{g(1)}$  peak is related to O—Ti—O bending type, wherein only Ti moves and the oxygen movement remains fixed. In the case of ( $A_{1g}$  +  $B_{1g}$ ) vibration peak, it includes the movement of only oxygen atom with Ti remains fixed.

The Raman spectra of Au/Ag NPs loaded TiO<sub>2</sub> NWs samples are identical to that of the pure TiO<sub>2</sub> NWs, which clearly indicated that the TiO<sub>2</sub> retained its structure after incorporation of these metals. Au/Ag NPs related signals were not identified because of the relatively low concentrations and due to the weak Raman scattering of these metals [41]. However, changes are obvious in the position and width of the Au/Ag NPs modified TiO<sub>2</sub> peaks. With the loading of Au and Ag NPs, the Raman band  $E_{g(1)}$  is slightly shifted toward higher wavenumber, Raman band  $B_{1g}$  and  $E_{g(3)}$  was broadened but their intensities were reduced. This indicated that the interaction between Au/Ag NPs and TiO<sub>2</sub> [42]. On the other hand, ( $A_{1g}$  +  $B_{1g}$ ) vibration peak disappeared in both Au and Ag loaded TiO<sub>2</sub> NWs samples, probably due to less movement of oxygen atom in the presence of these metals NPs over the TiO<sub>2</sub> NWs structure. Furthermore, Au-Ag co-coated TiO<sub>2</sub> NWs have the similar reflection as that of the pure TiO<sub>2</sub> NWs, confirming anatase phase of TiO<sub>2</sub>. More importantly, a distinct peak appeared at 897 cm<sup>-1</sup> by the presence of Au-Ag co-metals in the TiO<sub>2</sub> NWs, probably due to the formation of Au-Ag alloy. These observations have confirmed successful deposition of the Au-Ag alloy over the TiO<sub>2</sub> surface without any phase transition.

Fig. 3 exhibits FESEM images and DEX analysis of the pure TiO<sub>2</sub> NWs and Au/Ag NPs loaded TiO<sub>2</sub> NWs. Fig. 3(a) depicts TiO<sub>2</sub> NWs are uniform in length and no bundles of wires were observed. The EDX analysis in Fig. 3(b) shows the presence of Ti and O elements in the TiO<sub>2</sub>. Fig. 3(c) and (e) depicts the presence of Ag-NPs and Au-NPs over the TiO<sub>2</sub> NWs. It can be observed that Ag-NPs and Au-NPs are entirely distributed over the surface of TiO<sub>2</sub> NWs. The EDX analysis of Ag-NPs and Au-NPs is presented in Fig. 3(d) and (f), confirming the presence of Ag and Au metals over the TiO<sub>2</sub> surface. The Au-Ag NPs co-loading with uniform distribution could be seen in Fig. 3(g). The presence of both Ag and Au NPs can be observed in Fig. 3(h). Noticeably, both metals can be evenly spread over the TiO<sub>2</sub> surface using chemical reduction and photo-deposition method.

The deposition of Au/Ag NPs was further investigated using high resolution TEM as shown in Fig. 4. TEM images in Fig. 4(a) and (c) clearly show the uniform distribution of Au/Ag NPs over the TiO<sub>2</sub> NWs surface. The TiO<sub>2</sub> NWs detected are different sizes with diameters in the range of 17–70 nm. Fig. 4(b) displays the particle size distribution of Au/Ag NPs in the range of 3–100 nm with a mean value of 20 nm. The large size Au/Ag NPs coated over the TiO<sub>2</sub> NWs were observed due to Au-Ag alloy formation. However, the amounts of large size Au-Ag alloy NPs existing in the sample are less than the separated plasmonic Au and Ag NPs. More impor-



**Fig. 3.** FESEM images and EDX analysis of  $\text{TiO}_2$  NWs and Au/Ag loaded  $\text{TiO}_2$  NWs samples: (a) SEM image of  $\text{TiO}_2$  NWs, (b) EDX analysis of  $\text{TiO}_2$  NWs, (c) SEM image of Ag-NPs/ $\text{TiO}_2$  NWs, (d) EDX analysis of Ag-NPs/ $\text{TiO}_2$  NWs, (e) SEM image of Au-NPs/ $\text{TiO}_2$  NWs, (f) EDX analysis of Au-NPs/ $\text{TiO}_2$  NWs, (g) SEM image of Au/Ag NPs/ $\text{TiO}_2$  NWs, (h) EDX analysis of Au-Ag NPs/ $\text{TiO}_2$  NWs.

tantly, the smaller size Au and Ag NPs are also presented over the  $\text{TiO}_2$  NWs surface which can serve as electrons sink to promote the charges separation. The HR-TEM was used to investigate the crystal structure of the Au/Ag NPs supported  $\text{TiO}_2$  NWs, as shown in Fig. 4(d). The  $d$ -spacing of 0.35 nm reveals well the anatase  $\text{TiO}_2$  (101) plane, as already investigated by XRD and Raman analysis.

The  $\text{N}_2$ -adsorption-desorption isotherms of the pure  $\text{TiO}_2$ ,  $\text{TiO}_2$  NWs and Au/Ag-NPs modified  $\text{TiO}_2$  NWs samples are depicted in Fig. 5. The isotherms of all the samples are similar to the type IV curve with the hysteresis loops which is the characteristics of mesoporous materials. The summary of BET surface area, pore volume

and pore diameter of the  $\text{TiO}_2$ ,  $\text{TiO}_2$  NWs and modified  $\text{TiO}_2$  NWs samples is depicted in Table 1. BET specific surface area ( $S_{\text{BET}}$ ) of the pure  $\text{TiO}_2$  was 42 increased to  $75 \text{ m}^2 \text{ g}^{-1}$  for  $\text{TiO}_2$  NWs. On the other hand, BET surface area decreased to 46 and  $48 \text{ m}^2 \text{ g}^{-1}$  when 0.5 wt.% Au-NPs and 3 wt.% Ag-NPs were loaded onto  $\text{TiO}_2$  NWs. This decreased in the BET surface area could be accounted for partial  $\text{TiO}_2$  NWs surface covered by the deposited of metal NPs. However, an increased in BET surface area was observed in Au/Ag-NPs co-loaded  $\text{TiO}_2$  NWs. This increased in BET surface area was evidently due to the Au-Ag alloy supported over the  $\text{TiO}_2$  NWs. Similar observations were obtained in BJH adsorption pore volumes. In the case

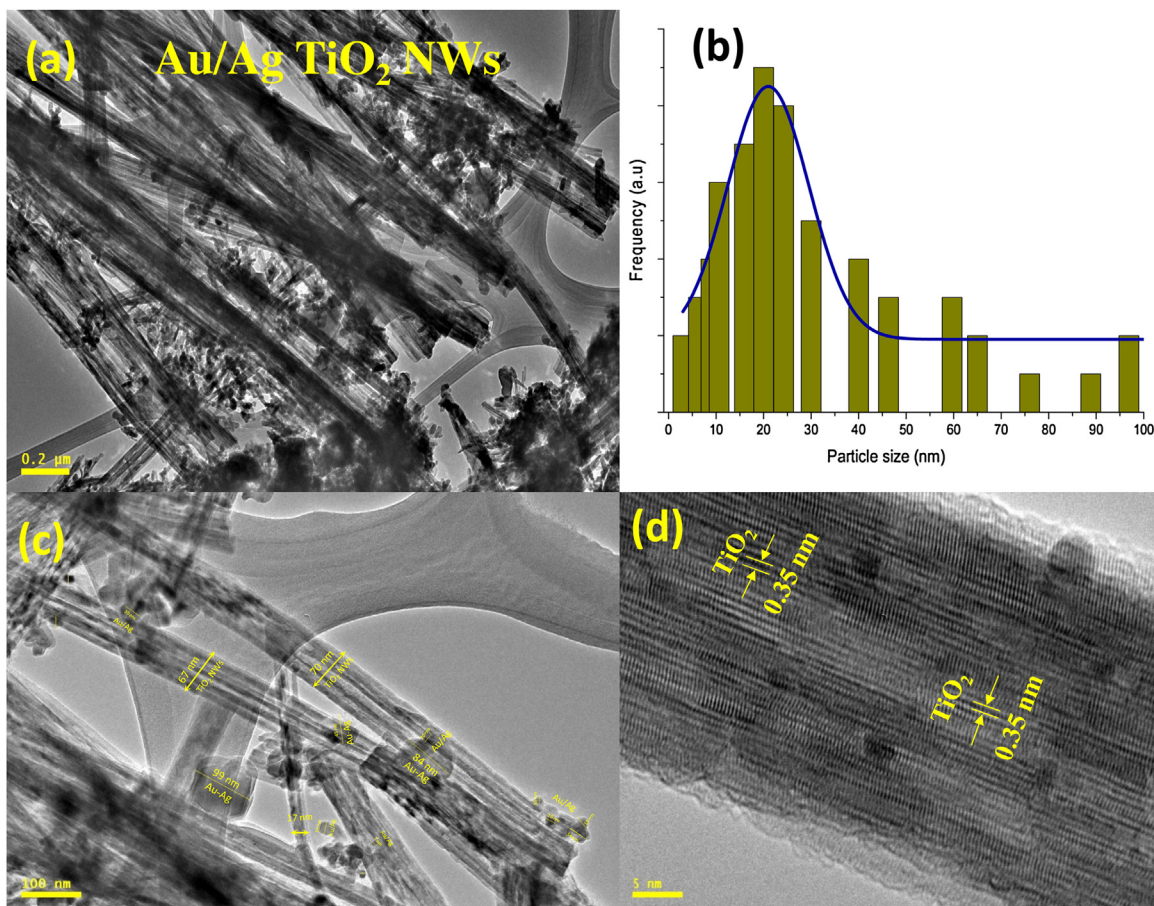


**Fig. 4.** TEM images of Au/Ag NPs supported TiO<sub>2</sub> NWs and their size distribution: (a and c) TEM images of Au/Ag-NPs/TiO<sub>2</sub> NWs at different magnification, (b) Au/Ag NPs size distribution over the TiO<sub>2</sub> NWs, (d) HR-TEM images with d-spacing of corresponding sample.

**Table 1**  
Summary of physiochemical characteristics of  $\text{TiO}_2$ ,  $\text{TiO}_2$  NWs and Au/Ag-NPs modified  $\text{TiO}_2$  NWs samples.

Type of catalyst	BET surface area(m <sup>2</sup> /g)	BJH adsorption pore volume(cm <sup>3</sup> /g)	BJH pore diameter(nm)	Band gap energy(eV)
TiO <sub>2</sub>	42	0.15	10	3.12
TiO <sub>2</sub> NWs	75	0.64	26	3.15
0.5% Au/TiO <sub>2</sub> NWs	46	0.43	34	3.11
3% Ag/TiO <sub>2</sub> NWs	48	0.49	32	3.13
2% Ag-0.5% Au/TiO <sub>2</sub> NWs	78	0.63	38	3.11

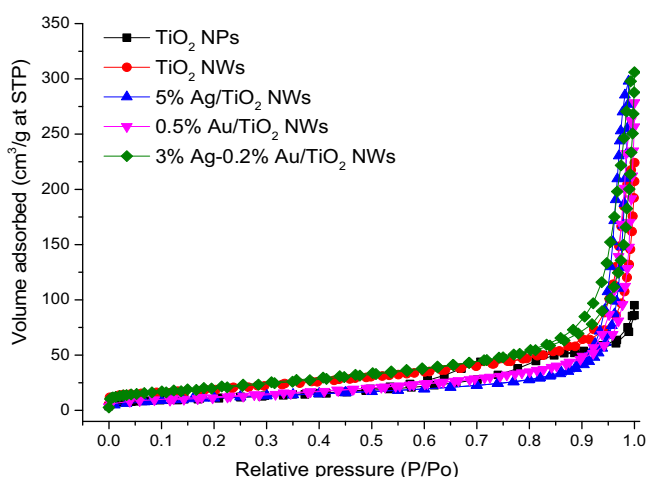


**Fig. 5.**  $N_2$  adsorption-desorption isotherms of  $TiO_2$  NPs,  $TiO_2$  NWs and Au/Ag deposited  $TiO_2$  NWs samples.

of pore diameter, pure  $\text{TiO}_2$  pore diameter was 10 nm, increased to 26 nm in  $\text{TiO}_2$  NWs, apparently due to the larger diameter of  $\text{TiO}_2$  NWs. A further increased in the pore diameter was observed in Au/Ag NPs loaded  $\text{TiO}_2$  NWs seemingly due to deposited Au/Ag-NPs layer over the surface of these materials [31].

X-ray photo-electron spectroscopy (XPS) was used to analyze the chemical states of the elements in Au/Ag-NPs/TiO<sub>2</sub> NWs as shown in Fig. 6. The wide spectrum is presented in Fig. 6(a). Fig. 6(b) reveals the presence of Ti2p peaks namely Ti2p 3/2 and Ti2p 1/2, positioned at 458.08 and 463.72 eV which corresponds to Ti<sup>4+</sup> or titanium dioxide (TiO<sub>2</sub>). The Ag3d spectrum confirmed the presence of Ag in the metal state as depicted in Fig. 6(c) [21]. Fig. 6(d) presents Au 4f binding energy values of 82.03 eV (Au 4f<sub>7/2</sub>) and 88.44 eV (Au 4f<sub>5/2</sub>) in Au-Ag/TiO<sub>2</sub> NWs, attributed to metallic gold (Au<sup>0</sup>). Fig. 6(e) shows the O1s spectrum ascribed to the lattice oxygen O<sub>2</sub>. This was also due to the presence of H<sub>2</sub>O or the free hydroxyl group (O-H) on the TiO<sub>2</sub> surface. The spectrum of C 1s with peaks located at ~284.60 and 588.50 eV corresponds to C-C, and C=O, respectively as shown in Fig. 6(f).

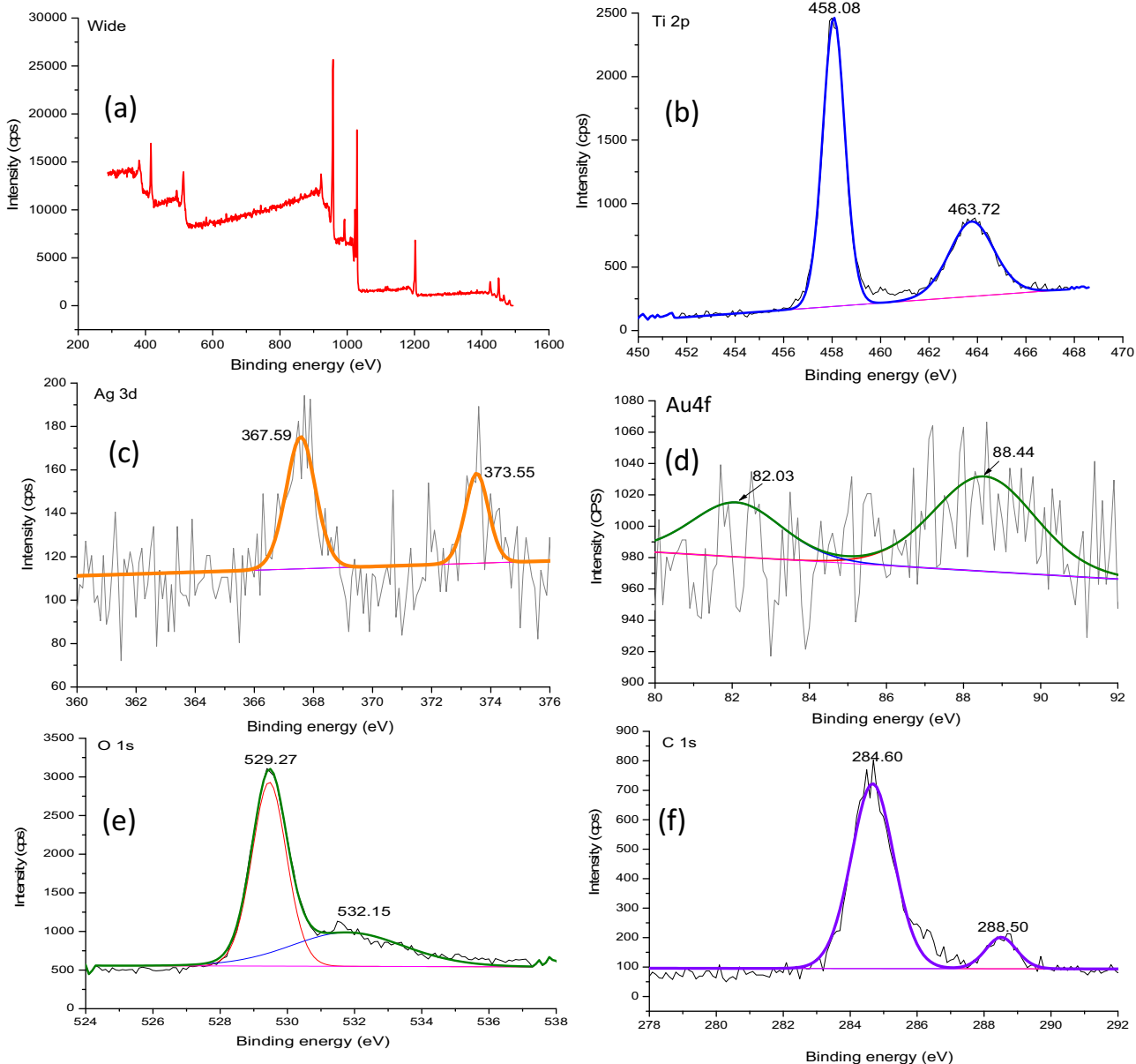


**Fig. 6.** XPS the spectra of 2 wt.% Ag–0.5 wt.% Au/TiO<sub>2</sub> NWs photocatalyst: (a) wide plot, (b) Ti 2p, (c) Ag-3d, (d) Au-4f, (e) O1s and C 1s.

The UV-vis diffuse reflectance absorbance spectra of the TiO<sub>2</sub> NWs and plasmonic Au/Ag loaded TiO<sub>2</sub> NWs samples are presented in Fig. 7(a). Both Au-NPs and Ag-NPs loaded into TiO<sub>2</sub> NWs revealed a broad visible light absorption peak due to LSPR absorption of Au-NPs and Ag-NPs, indicating metallic Au and Ag exists over the TiO<sub>2</sub> NWs surface as recognized by XPS. The LSPR peak of Ag-NPs appeared at 576 nm compared to its standard peak position of 450 nm. This red shift in peak toward longer wavelength was most likely due to the large size Ag-NPs with face centered cubic (fcc) structure of Ag [43–45]. However, Au-NPs give standard reflection with peak located at 580 nm due to LSPR of Au-NPs. On the other hand, the overlap between the plasmon resonance of 3% Ag–0.5% Au loaded TiO<sub>2</sub> NWs (around 450–700 nm) appeared and makes it difficult to see the individual response of both metals. The LSPR peak of Au/Ag NPs supported TiO<sub>2</sub> NWs was further broadened (around 410–750 nm) by loading 2% Ag and 0.5% Au into TiO<sub>2</sub> NWs. This, single broadened LSPR peak in the spectrum of Au/Ag NPs could probably be due to Au-Ag alloy formation, in good agreement with the previous reports [37,46]. More importantly, the illuminations

due to LSPR of Au/Ag NPs could be seen when the samples were excited with a laser beam of wavelength 532 nm, as depicted in Fig. 7(b–d). The emitting of light due to LSPR of Au and Ag NPs could be seen in Fig. 7(b–c). However, the obvious light glowing spots in the Au/Ag NPs co-coated TiO<sub>2</sub> NWs sample is evidently due to the Au-Ag alloy formation and less bright areas were due to the Au/Ag NPs co-coated over TiO<sub>2</sub> NWs as depicted in Fig. 7(d). These observations have confirmed the formation of Au-Ag alloy and gave strong LSPR response due to synergistic effect in Au/Ag metals.

Fig. 8 shows PL emission spectra of the pure TiO<sub>2</sub> NWs and Au/Ag-NPs modified TiO<sub>2</sub> NWs samples excited at a wavelength of 532 nm. The broad symmetric peaks appeared at 536 nm revealed that the emission is not because of TiO<sub>2</sub> band edge excitation [8]. Therefore, PL signals can be attributed to the transition of electrons from the oxygen vacancies to TiO<sub>2</sub> valence band. It is noticeable that emission spectra of the Au and Ag modified TiO<sub>2</sub> samples are similar to those of the pure TiO<sub>2</sub> NWs sample. However, the PL intensity enfeebled in Au-NPs and Ag-NPs sample and further reduced in

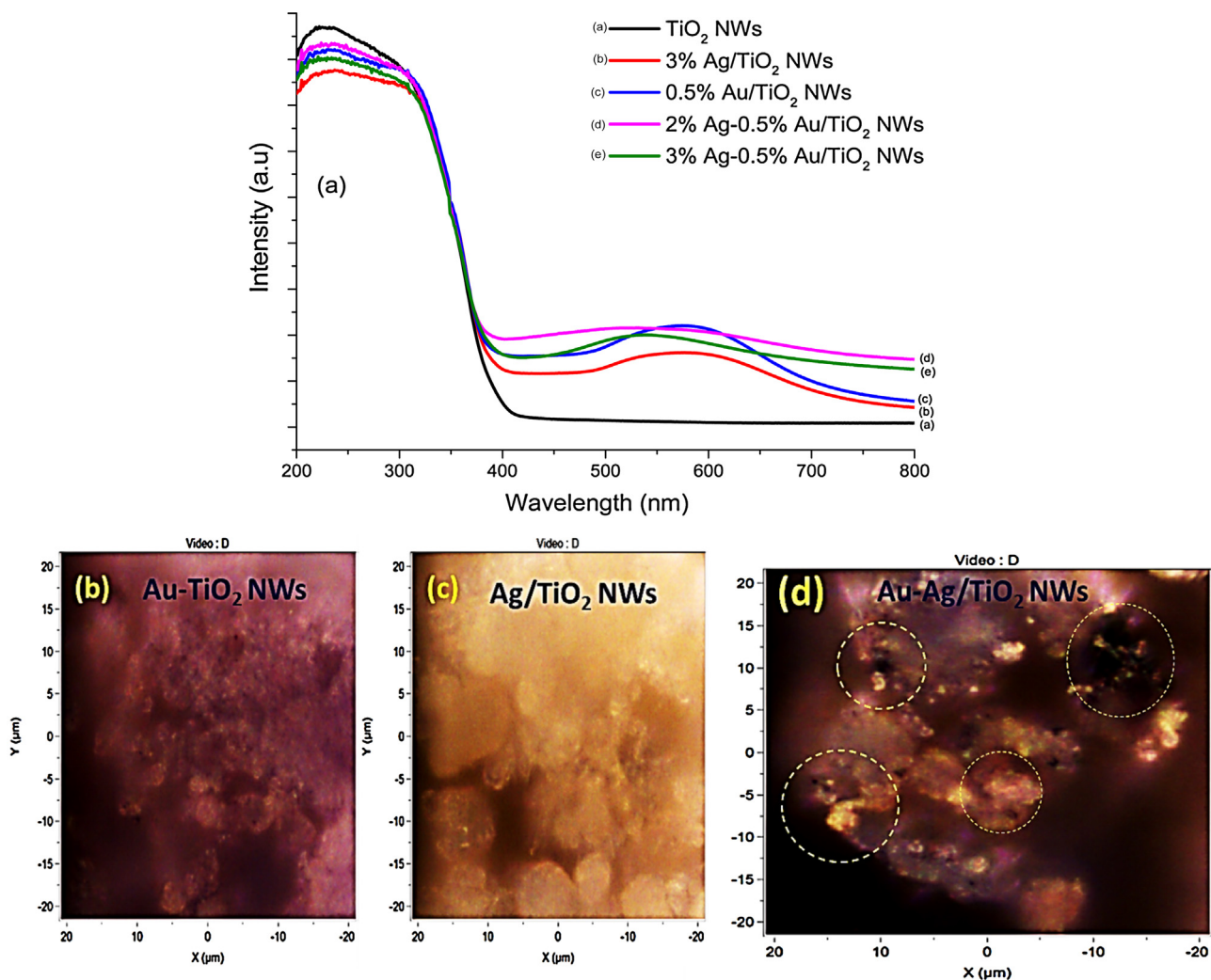


**Fig. 7.** (a) UV-vis diffuse reflectance spectra of  $\text{TiO}_2$  NPs,  $\text{TiO}_2$  NWs and Au/Ag-NPs loaded  $\text{TiO}_2$  NWs, (b-d) Photographs of the illuminations of powder photocatalysts due to LSPR of Au/Ag NPs excited with a laser beam of wavelength 532 nm.

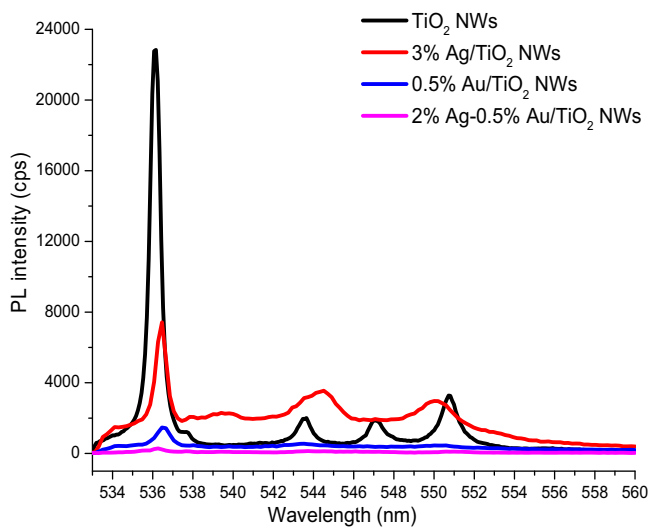


**Fig. 8.** Photoluminescence spectra of  $\text{TiO}_2$  and Au/Ag NPs loaded  $\text{TiO}_2$  samples.

Au/Ag NPs co-loaded  $\text{TiO}_2$  NWs samples. The electron transfers from the  $\text{TiO}_2$  NWs to Au/Ag promoted  $\text{TiO}_2$  NWs are more effi-

cient than the single metal loaded  $\text{TiO}_2$  NWs, confirming synergistic effects of these metals in  $\text{TiO}_2$  NWs surface.

### 3.2. Photocatalytic $\text{CO}_2$ reduction with $\text{H}_2$

Prior to  $\text{CO}_2$  photoreduction activity test, a series of preliminary tests were conducted in the absence of reductants ( $\text{CO}_2$ ,  $\text{H}_2$ ) over all types of photocatalysts. In all cases, reaction products were not detected, confirming no organic residues in the catalyst. Additional preliminary tests were conducted using  $\text{H}_2$  in presence of photocatalyst under light irradiations. Again, carbon containing compounds were not observed. However, a significant amount of CO was produced during  $\text{CO}_2$  reduction with  $\text{H}_2$  under the light irradiations in the presence of photocatalyst. These results have confirmed that the photoreduction products were obtained from the  $\text{CO}_2$  source only. All the photocatalytic  $\text{CO}_2$  reduction experiments were repeated at least in triplets and aggregated results have been reported.

The effects of Ag-NPs, Au-NPs and Au/Ag-NPs on the performance of  $\text{TiO}_2$  NWs for photocatalytic  $\text{CO}_2$  reduction with  $\text{H}_2$  in the production of CO,  $\text{CH}_3\text{OH}$  and hydrocarbons under visible light irradiation are demonstrated in Figs. 9 and 10. Fig. 9 shows the effect of Ag-NPs and Au-NPs on the photoactivity of  $\text{TiO}_2$  NWs for the production of CO as the main product with a smaller amount of hydrocarbons. We noted that in the absence of Ag/Au NPs, only

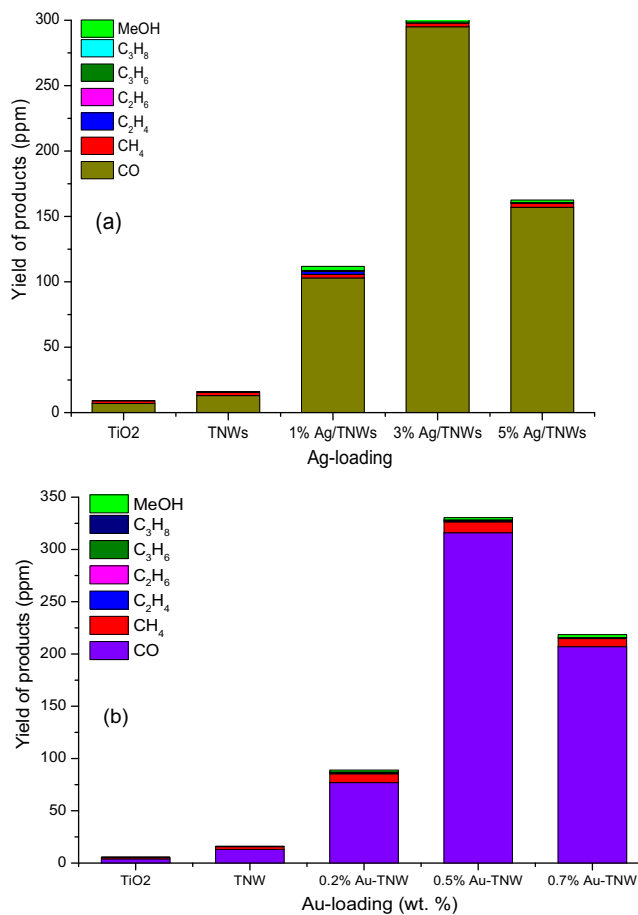


**Fig. 9.** Effect of Ag and Au NPs loading onto TiO<sub>2</sub> NWs photoactivity for CO, CH<sub>3</sub>OH and hydrocarbons production during CO<sub>2</sub> reduction with H<sub>2</sub>: (a) Ag-NPs loading, (b) Au-NPs loading.

smaller amount of CO was produced. However, a significant amount of CO production over TiO<sub>2</sub> NWs could be seen in the presence of Ag-NPs and Au-NPs. The pure TiO<sub>2</sub> and TiO<sub>2</sub> NWs have very low CO production because of their photoactivity only under the UV-light irradiations and perhaps due to fast recombination rate of photo-generated charge carrier. In contrast, Ag-NPs and Au-NPs decorated TiO<sub>2</sub> NWs exhibits much higher CO production rate with appreciable amounts of CH<sub>3</sub>OH and hydrocarbons. This is because Ag-NPs and Au-NPs in TiO<sub>2</sub> NWs act as an electrons sink to suppress charges recombination rate. On the other hand, by contacting Ag-NPs and Au-NPs with TiO<sub>2</sub> NWs, the plasmon-excited electron can be injected into TiO<sub>2</sub> and makes it visible light active, while smaller size metal particles could serve as electron sink, resulting in prolonged recombination time. In this way, an immediate charges separation can be attained on the metal-semiconductor surface to enhance photoactivity. The optimal Ag-NPs and Au-NPs loading were found to be 3 wt.% and 0.5 wt.%, respectively, at which highest yield of products were detected. However, with higher metals-loading, the photoactivity was gradually was reduced, possibly metals-NPs were adjacent to each other over TiO<sub>2</sub> NWs, creating recombination centers and electron-hole charges recombine immediately, resulting in lower photoactivity [21].

To evaluate the synergistic effects of Ag-NPs and Au-NPs, the TiO<sub>2</sub> NWs photoactivity was further evaluated in the presence of co-decorated Ag/Au NPs. The performance analysis of Au/Ag-NPs co-deposited on the TiO<sub>2</sub> NWs for photocatalytic CO<sub>2</sub> reduction with H<sub>2</sub> to CO is presented in Fig. 10(a). Interestingly, the CO production rate was remarkably enhanced using Au/Ag NPs co-loading

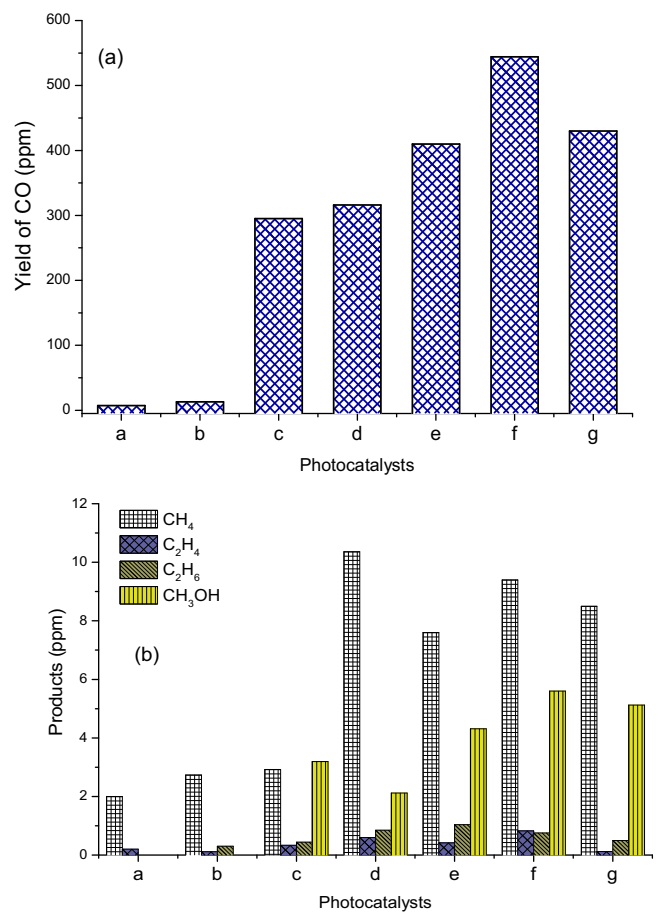


**Fig. 10.** Effect of Au/Ag-NPs co-loading onto TiO<sub>2</sub> photoactivity for CO and hydrocarbons production: (A) CO productions over photocatalysts (a) TiO<sub>2</sub>, (b) TNWs, (c) 3% Ag-TNWs, (d) 0.5% Au-TNWs, (e) 1% Ag-0.5% Au/TNWs, (f) 2% Ag-0.5% Au/TNWs, (g) 3% Ag-0.5% Au/TNWs; (B) Methanol and hydrocarbons production over the corresponding photocatalysts.

as compared to Ag-NPs or Au-NPs. This suggests that synergistic effects, alloy formation optical responses (e.g. LSPR) and electrons sink of Au/Ag NPs over the TiO<sub>2</sub> NWs must play a crucial role in the production of CO and other products [35]. Evidently, all the Ag-NPs decorated Au-NPs/TiO<sub>2</sub> NWs photocatalysts demonstrated excellent performances for selective photoreduction of CO<sub>2</sub> to CO over the single metal-ions loaded TiO<sub>2</sub> NWs. The highest CO production was noticed over 2 wt.% Ag-NPs loaded into the fixed amounts of 0.5 wt.% Au-NPs/TiO<sub>2</sub> NWs, which showed the optimal loading. It is noticeable to see that the optimal amount of Ag-NPs-loading in the pure TiO<sub>2</sub> NWs was 3 wt.%, while only 2 wt.% Ag-NPs loaded into 0.5 wt.% Au-NPs/TiO<sub>2</sub> NWs gave the optimal photoactivity. This revealed that Au/Ag NPs co-loading over the TiO<sub>2</sub> NWs significantly improved photoactivity toward CO evolution due to their synergistic effects.

The production of hydrocarbons and CH<sub>3</sub>OH over Au/Ag NPs coated TiO<sub>2</sub> NWs are presented in Fig. 10(b). Using pure TiO<sub>2</sub> and TiO<sub>2</sub> NWs, production of CH<sub>3</sub>OH was not detected, yet loading of both Au-NPs and Ag-NPs have favored production of CH<sub>3</sub>OH and hydrocarbons. The production of CH<sub>3</sub>OH was highest in the Au/Ag co-coated TiO<sub>2</sub> NWs samples, however, Au-NPs/TiO<sub>2</sub> NWs favored CH<sub>4</sub> production. Among the hydrocarbons, a significant amount of C<sub>2</sub>H<sub>6</sub> was detected in the products mixture with appreciable amount of C<sub>2</sub>H<sub>4</sub>. The methanol and hydrocarbons production was significant using Au/Ag-NPs co-loading TiO<sub>2</sub> NWs samples, evidently due to Au-Ag alloy with absorption of broader light spectrum

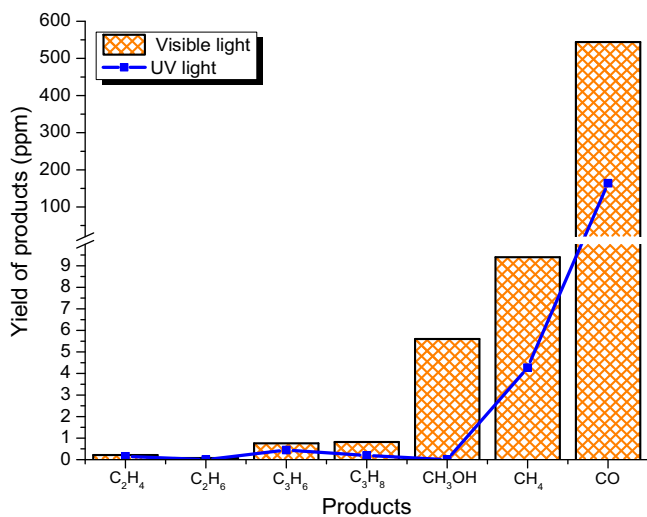


**Fig. 11.** Performance analysis of Au-Ag NPs supported  $\text{TiO}_2$  NWs under UV and visible light irradiations.

and LSPR-excitation of  $\text{TiO}_2$  NWs with electron sinks by these metals toward  $\text{CO}_2$  reduction.

The effects of UV and visible light irradiations on the activity of plasmonic 2 wt.% Ag–0.5 wt.% Au-NPs loaded  $\text{TiO}_2$  NWs for photo-induced  $\text{CO}_2$  reduction to CO and hydrocarbons are demonstrated in Fig. 11. Obviously, the production of CO,  $\text{CH}_3\text{OH}$  and hydrocarbons was significant using visible-light-irradiations compared to UV-light under the same operating conditions. The amount of CO produced under visible-light was 3.28 fold more than using UV-light and similar trends could be seen for the production of hydrocarbons. More importantly, an appreciable amount of  $\text{CH}_3\text{OH}$  was also detected using visible light irradiations but was not detected with UV-light source. More importantly, the light intensity of UV-light ( $150 \text{ mW cm}^{-2}$ ) was more stronger than the visible light irradiations ( $20 \text{ mW cm}^{-2}$ ), yet the significantly enhanced photoactivity of Au/Ag NPs Co-loaded  $\text{TiO}_2$  NWs toward  $\text{CO}_2$  reduction was evidently due to synergistic effects between broad spectrum of visible light absorption by Au-Ag alloy and efficient electron separation by Au/Ag NPs.

The summary of yield rates and selectivity of different products over the various  $\text{TiO}_2$  based catalysts during photocatalytic  $\text{CO}_2$  reduction with  $\text{H}_2$  as reducing agent under visible light irradiations are presented in Fig. 12 and tabulated in Table 2. The  $\text{CO}_2$  reduction products observed were CO,  $\text{CH}_3\text{OH}$ ,  $\text{CH}_4$ ,  $\text{C}_2\text{H}_4$ ,  $\text{C}_2\text{H}_6$ ,  $\text{C}_3\text{H}_6$  and  $\text{C}_3\text{H}_8$  over different types of photocatalysts. The pure  $\text{TiO}_2$  NPs and  $\text{TiO}_2$  NWs show poor photoactivity for  $\text{CH}_3\text{OH}$  but found more efficient toward CO production. The photoactivity of  $\text{CO}_2$  reduction was gradually increased using  $\text{TiO}_2$  NWs than the  $\text{TiO}_2$  NPs. This was conceivably due to effectual electron transfer over the  $\text{TiO}_2$  NWs than the  $\text{TiO}_2$  NPs. In comparison, the Au-NPs/ $\text{TiO}_2$  NWs displays 1.07 times higher photoactivity for CO production than the Ag-NPs/ $\text{TiO}_2$ . This was because instead of LSPR function of Au-NPs, they are good electron acceptors to promote charges separation on the  $\text{TiO}_2$  surface because of strong oxidation and reduction potentials in the Au-metal, as discussed in our previous work [47]. This was because of the higher electrons sink effect of the Au-NPs than the Ag-NPs due to its lower work function than the Ag-NPs, resulting in efficient separation of photo-generated charges. Therefore, multi-electron process would occur more efficiently over the Au-NPs than the Ag-NPs based  $\text{TiO}_2$  NWs. However, the production of CO was significantly enhanced using Au/Ag NPs co-promoted  $\text{TiO}_2$  NWs due to synergistic effects between Au-Ag alloy NPs, efficient visible light absorption, LSPR excitation of  $\text{TiO}_2$  NWs, efficient

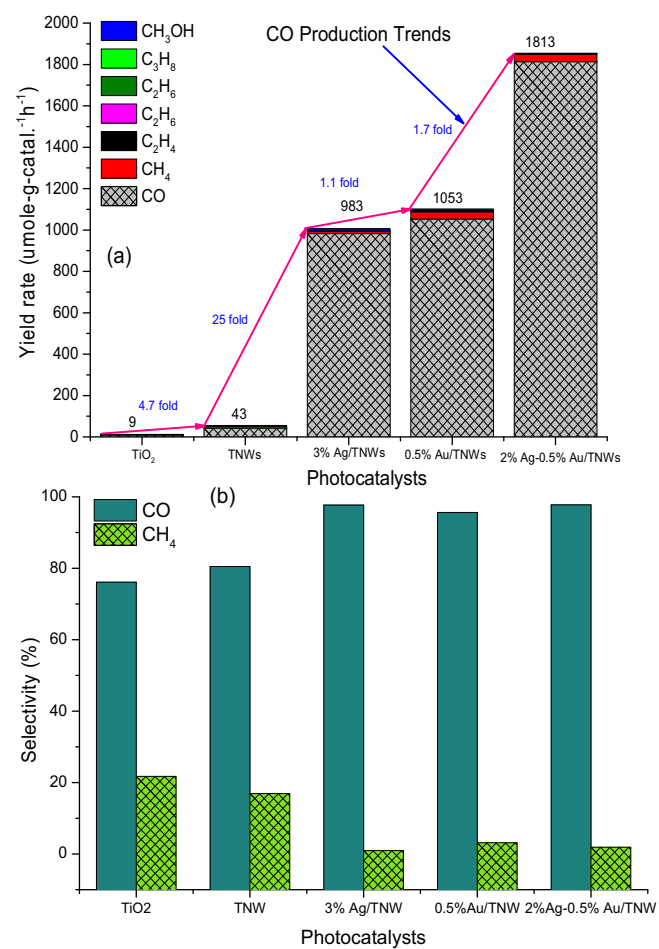


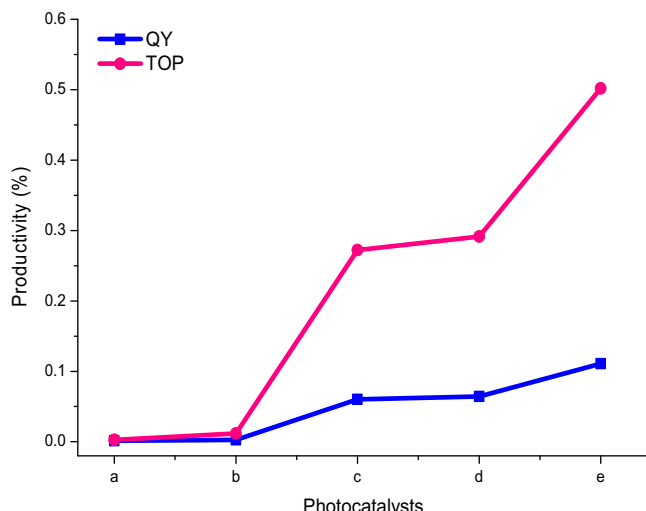
**Fig. 12.** (a) Yield rate of products over different photo-catalysts during  $\text{CO}_2$  reduction with  $\text{H}_2$ ; (b) Selectivity of CO and  $\text{CH}_4$  for corresponding samples.

charge transfer property and hindered charges recombination rate by Au/Ag NPs.

The yield rate of CO over the Au/Ag-NPs loaded  $\text{TiO}_2$  NWs was  $1813 \text{ }\mu\text{mole g-catal.}^{-1} \text{ h}^{-1}$  which was higher than the Au-NPs/ $\text{TiO}_2$  NWs ( $1053 \text{ }\mu\text{mole g-catal.}^{-1} \text{ h}^{-1}$ ), Ag-NPs/ $\text{TiO}_2$  NWs ( $983 \text{ }\mu\text{mole g-catal.}^{-1} \text{ h}^{-1}$ ),  $\text{TiO}_2$  NWs ( $43 \text{ }\mu\text{mole g-catal.}^{-1} \text{ h}^{-1}$ ) and un-doped  $\text{TiO}_2$  ( $9 \text{ }\mu\text{mole g-catal.}^{-1} \text{ h}^{-1}$ ). This comparison demonstrated that the decoration of Ag/Au-NPs on the  $\text{TiO}_2$  NWs structure enables great enhancement of photocatalytic efficiency through the LSPR-excitation of Au-Ag alloy or one of the metals (e.g. Au-NPs) and electron sink by the other metal (e.g. Ag-NPs), simultaneously. The yield rate of  $\text{CH}_4$  production was higher in the order of Au/Ag/ $\text{TiO}_2$  NWs > Au/ $\text{TiO}_2$  NWs > Ag/ $\text{TiO}_2$  NWs >  $\text{TiO}_2$  NWs >  $\text{TiO}_2$ . The  $\text{CH}_3\text{OH}$  production was detected only over Au-NPs and Ag-NPs loaded  $\text{TiO}_2$  NWs. However, much higher CO production over Au/Ag-NPs/ $\text{TiO}_2$  NWs was obviously due to higher electron mobility with hindered recombination rate and LSPR effect of Au/Ag-NPs. The selectivity for CO production over  $\text{TiO}_2$  NWs was 80%, increased to 97% in Au/Ag-NPs co-loaded  $\text{TiO}_2$  NWs. This increased in selectivity was due to efficient photo-induced  $\text{CO}_2$  to CO conversion over plasmonic Au/Ag NPs promoted  $\text{TiO}_2$  catalysts. These observations have confirmed that the RWGS reaction is favorable for  $\text{CO}_2$  reduction by  $\text{H}_2$  to CO due to LSPR of Au/Ag NPs in  $\text{TiO}_2$  NWs [13,47]. Furthermore, stability and reusability test of Au/Ag-NPs co-deposited  $\text{TiO}_2$  NWs for photocatalytic  $\text{CO}_2$  reduction with  $\text{H}_2$  through a cycling run was conducted. There was no obvious decrease of the photoactivity of Au/Ag-NPs-loaded  $\text{TiO}_2$  after three cyclic runs, demonstrating the good stability of this photo-catalyst.

**Table 2**Summary of yield rate of  $\text{CO}_2$  photo-reduction over  $\text{TiO}_2$ ,  $\text{TiO}_2$  NW and Au/Ag-deposited  $\text{TiO}_2$  NWs photocatalysts.

Catalysts	Production rate		$(\mu\text{mole g-catal.}^{-1} \text{h}^{-1})$					Selectivity (%)	CO (%)	CH <sub>4</sub> (%)
	CO	CH <sub>4</sub>	C <sub>2</sub> H <sub>4</sub>	C <sub>2</sub> H <sub>6</sub>	C <sub>3</sub> H <sub>6</sub>	C <sub>3</sub> H <sub>8</sub>	CH <sub>3</sub> OH			
$\text{TiO}_2$	9	3.0	0.27	–	–	–	–	76.09	21.74	
$\text{TiO}_2$ NWs	43	9	0.38	1.01	–	–	–	80.50	16.93	
0.5% Au-NPs/ $\text{TiO}_2$ NWs	1053	30	1.99	2.83	0.44	1.23	7.07	95.63	3.14	
3% Ag-NPs/ $\text{TiO}_2$ NWs	983	10	1.11	1.48	0.23	1.12	10.65	97.72	0.97	
2% Ag–0.5% Au/ $\text{TiO}_2$ NWs	1813	35	0.95	2.52	3.94	3.52	18.76	97.70	1.86	

**Fig. 13.** Plot of quantum yield and turn over productivity for CO production over different photo-catalysts: (a)  $\text{TiO}_2$ , (b)  $\text{TiO}_2$  NWs, (c) 3% Ag/ $\text{TiO}_2$  NWs, (d) 0.5% Au/ $\text{TiO}_2$  NWs, (e) 2% Ag–0.5% Au/ $\text{TiO}_2$  NWs.

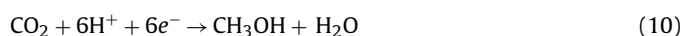
It is generally accepted that the photocatalyst efficiency is mainly dependent on the light absorption ability, surface properties (e.g., specific surface area, pore structure, pore volume, adsorption property etc.) and photo-generated electron/hole pairs separation efficiency. It is evidenced that photoactivity for CO evolution rate over the  $\text{TiO}_2$  NWs can be improved by 23 fold over 3 wt.% Ag-NPs loading and 25 fold by 0.5 wt.% Au-loading. However, as discussed above the  $\text{TiO}_2$  NWs surface area is much higher than the Au-NPs and Ag-NPs loaded  $\text{TiO}_2$  NWs, indicating that in the current study, this factor is not crucial to the photocatalytic activity for Au-NPs and Ag-NPs/ $\text{TiO}_2$  NWs. The enhanced photocatalytic activity can be mainly attributed to surface plasmon resonance of Au-NPs and Ag-NPs. More importantly, the surface area of  $\text{TiO}_2$  NWs and Au-Ag-NPs/ $\text{TiO}_2$  NWs are much closer, yet CO production rate over 2 wt.% Ag–0.5 wt.% Au-co-loading  $\text{TiO}_2$  NWs was 42 fold more than the amount produced over the pure  $\text{TiO}_2$  NWs. Therefore, this significantly enhanced photocatalytic activity of Au/Ag NPs co-coated  $\text{TiO}_2$  NWs mainly attributed to strong visible light absorption due to surface plasmon resonance of Au-Ag alloy and synergistic effect between Au/Ag-NPs. This can greatly promote the production and separation of photo-generated carriers under the broader visible light spectrum.

The quantum yield was calculated based on 2 electrons used for CO production and moles of photons input energy over the catalyst surface. The quantum yields (QY) and turn over productivity (TOP) of CO over  $\text{TiO}_2$  NWs and Au/Ag-NPs loaded are shown in Fig. 13 and summarized in Table 3. The significantly enhanced QY could be seen over Au/Ag-NPs/ $\text{TiO}_2$  NWs compared to Au-NPs/ $\text{TiO}_2$  NWs, Ag-NPs/ $\text{TiO}_2$  NWs and pure  $\text{TiO}_2$  NWs. More importantly, TOP was more significant over Au/Ag NPs loaded  $\text{TiO}_2$  NWs compared to single-metal loaded  $\text{TiO}_2$  NWs and bare  $\text{TiO}_2$  NWs. This was evidently due to efficient charge transfer rate and SPR-excitation due

to synergistic effect of Au/Ag-NPs. It is evident that TOP is much higher than QY because it was calculated based on the operating parameters. The pressure has positive effects on TOP but reduced with increase of temperature and catalyst loading. However, QY is independent of these operating parameters which are very important in photocatalysis system. In different research work, results were reported at different catalyst loading and reaction temperature, yet the results were compared based on QY. Therefore, the performance of the photocatalytic system in gas phase system could be accurately compared based on TOP than the QY.

### 3.3. The mechanism of photocatalytic reaction

LSPR-induced photocatalytic reaction mechanism of  $\text{TiO}_2$  loaded with metal-NPs has been discussed in several reports [31,35]. The visible light can provide an energy transfer channel while the light captured by  $\text{TiO}_2$  NWs can be reused by Au-NPs resulting in enhanced LSPR effect. The LSPR-excitation of Au/Ag-NPs enhances visible light excitation through strong localized electric field and improves charge separation on  $\text{TiO}_2$  NWs [48]. Electrons can be injected from LSPR-excited by Au-Ag alloy or Au/Ag NPs toward  $\text{TiO}_2$  surface, captured by Au/Ag-NPs and subsequent reduction and oxidation reactions occur for  $\text{CO}_2$  and  $\text{H}_2$ , respectively. This synergistic effect in Au/Ag NPs over  $\text{TiO}_2$  NWs for LSPR-induced chemical reaction has been proposed as for the reaction mechanism. The overall proposed mechanism to understand the reaction process is illustrated in Eqs. (3)–(12) [22].

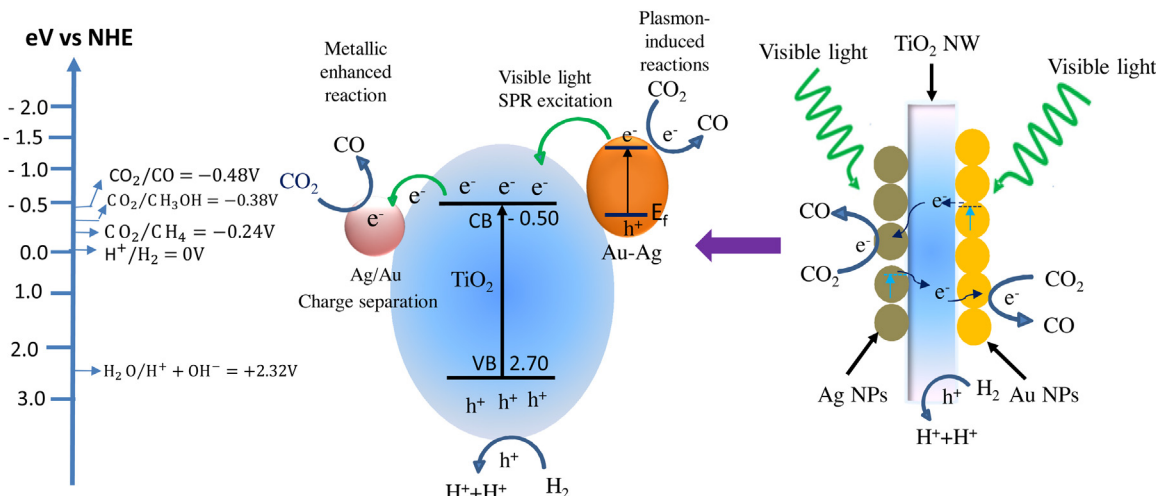


On the basis of above results and discussion,  $\text{CO}_2$  reduction and  $\text{H}_2$  oxidation over Au/Ag-NPs supported  $\text{TiO}_2$  NWs can be explained as follows: First, when the visible light was irradiated to Au/Ag-NPs/ $\text{TiO}_2$  NWs, photons were absorbed by the Au/Ag NPs due to the LSPR excitation as explained in Eqs. (3) and (4). The excited electrons in the Au/Ag are injected into the conductance band of  $\text{TiO}_2$  (Eq. (5)). The electrons are transferred toward Au/Ag metals, making them to react easily with  $\text{CO}_2$  as illustrated in Eqs. (6)–(7). The valence band holes are used to oxidize  $\text{H}_2$  for the production of hydrogen radicals (Eq. (8)). Then,  $\text{H}^+$  radicals and active electrons can reduce  $\text{CO}_2$  to CO,  $\text{CH}_3\text{OH}$  and  $\text{CH}_4$  as explained in Eqs. (9)–(11). CO production needs only two electrons and two protons (Eq. (9)).

**Table 3**

Summary of QY and TOP of CO production over various photocatalysts.

Catalysts	Yield of CO(μmole g-catal.⁻¹ h⁻¹)	QY (%)	TOP(%)
TiO <sub>2</sub>	9	0.0014	0.0025
TiO <sub>2</sub> NWs	43	0.0026	0.0119
3% Ag-TiO <sub>2</sub> NWs	983	0.0601	0.2721
0.5% Au-TiO <sub>2</sub> NWs	1053	0.0643	0.2915
2% Ag-0.5% Au-TiO <sub>2</sub> NWs	1813	0.1108	0.5018

**Fig. 14.** Proposed mechanism showing a photocatalytic process for CO<sub>2</sub> reduction by H<sub>2</sub> to CO on Au/Ag-NPs/TiO<sub>2</sub> NWs under visible light irradiation.

The production of CO as the main product was due to the proximity of thermodynamic difference between TiO<sub>2</sub> CB (−0.5 eV) and the reduction potential of CO<sub>2</sub>/CO (−0.48 eV). CH<sub>3</sub>OH and CH<sub>4</sub> can be produced directly through a multi-step reduction process which involved six and eight electrons and protons, respectively (Eqs. (10) and (12)). Besides, there would also be possible production of CH<sub>4</sub> by the depletion of as-produced CO through a six electron reaction involvement (Eq. (11)). Therefore, significantly enhanced photocatalytic activity by Au/Ag-decorated TiO<sub>2</sub> NWs can be explained based on synergistic effects and LSPR excitation.

The schematic presentation of plasmon-enhanced photocatalytic activity over the Au/Ag NPs co-promoted TiO<sub>2</sub> NWs is illustrated in Fig. 14. Upon LSPR excitation, the surface electron on Au/Ag NPs or Au-Ag alloy can be excited to a higher energy level where electrons are transferred to CB band of TiO<sub>2</sub> NWs through metals-TiO<sub>2</sub> NWs interfaces. At the same time, electron-hole separation of photo-excited TiO<sub>2</sub> may be promoted by smaller size Au/Ag NPs, which serves as electron sink and allows a longer lifetime of photo-generated electrons. In conclusions, the overall high photocatalytic activity of Au/Ag-NPs loaded TiO<sub>2</sub> NWs in solar fuels production can be attributed to efficient visible light absorption by Au-Ag alloy NPs, synergistic effects of LSPR excitation and electron sink of Au/Ag NPs.

#### 4. Conclusions

Au/Ag-NPs-co-decorated TiO<sub>2</sub> NWs have been successfully fabricated using a facile thermal and photo-deposition method. Plasmon-induced photocatalytic CO<sub>2</sub> reduction by H<sub>2</sub> over Au/Ag NPs-co-decorated TiO<sub>2</sub> NWs were successfully conducted under visible light irradiation. The photo-activity of Au-NPs/TiO<sub>2</sub> NWs was more than Ag-NPs/TiO<sub>2</sub> NWs, probably due to greater LSPR effects by Au-NPs. The Au/Ag NPs loaded onto TiO<sub>2</sub> NWs exhibited remarkably improved visible light photocatalytic activity for CO evolution as compared to TiO<sub>2</sub> NWs with only single metal deposition (Au-NPs/TiO<sub>2</sub> NWs and Ag-NPs/TiO<sub>2</sub> NWs). CO evolution rate

of Au/Ag-NPs/TiO<sub>2</sub> NWs was approximately 72.52 times more than the amount produced over the pure TiO<sub>2</sub> NWs. The amount of CO produced under visible-light was 3.28 fold more than the amount produced using UV-light irradiations. These enhanced photocatalytic activities through co-deposition of Au/Ag NPs are attributed to synergistic effects based on LSPR excitation and electrons sink of Au/Ag NPs. The turnover productivity revealed, operating parameters have great influences to improve photoactivity and products selectivity. Therefore, synergistic effect between charger transfer and placement-excitation of Au/Ag-NPs can greatly enhance the performance of TiO<sub>2</sub> NWs. Thus, co-deposition of plasmonic Au-Ag alloy and Au/Ag NPs could provide a more effective way to harvest solar energy over a broader range of solar spectrum.

#### Acknowledgements

The authors would like to extend their deepest appreciation to MOHE (Ministry of Higher Education) Malaysia for financial support of this research project under FRGS (Fundamental Research Grant Scheme, Vote 4F876).

#### References

- [1] X. Li, Z. Zhuang, W. Li, H. Pan, *Appl. Catal. A: Gen.* 429–430 (2012) 31–38.
- [2] M. Tahir, N.S. Amin, *Appl. Catal. A: Gen.* 493 (2015) 90–102.
- [3] L. Yuan, Y.J. Xu, *Appl. Surf. Sci.* 342 (2015) 154–167.
- [4] M. Tahir, N.S. Amin, *Appl. Catal. B: Environ.* 162 (2015) 98–109.
- [5] S.Y. Zhu, S.J. Liang, J.H. Bi, M.H. Liu, L.M. Zhou, L. Wu, X.X. Wang, *Green Chem.* 18 (2016) 1355–1363.
- [6] Y. Liu, S. Zhou, J.M. Li, Y.J. Wang, G.Y. Jiang, Z. Zhao, B. Liu, X.Q. Gong, A.J. Duan, J. Liu, Y.C. Wei, L.Q. Zhang, *Appl. Catal. B: Environ.* 168 (2015) 125–131.
- [7] S.-Q. Liu, S.-S. Zhou, Z.-G. Chen, C.-B. Liu, F. Chen, Z.-Y. Wu, *Catal. Commun.* 73 (2016) 7–11.
- [8] M. Tahir, B. Tahir, N.A.S. Amin, A. Muhammad, *Energy Convers. Manage.* 119 (2016) 368–378.
- [9] M. Tahir, N.S. Amin, *Chem. Eng. J.* 285 (2016) 635–649.
- [10] B. Tahir, M. Tahir, N.S. Amin, *Energy Convers. Manage.* 90 (2015) 272–281.
- [11] F. Gonell, A.V. Puga, B. Julián-López, H. García, A. Corma, *Appl. Catal. B: Environ.* 180 (2016) 263–270.
- [12] M. Tahir, N.S. Amin, *Energy Convers. Manage.* 76 (2013) 194–214.

- [13] M. Tahir, B. Tahir, *Appl. Surf. Sci.* 377 (2016) 244–252.
- [14] J. Hu, H. Li, Q. Wu, Y. Zhao, Q. Jiao, *Chem. Eng. J.* 263 (2015) 144–150.
- [15] Z.Q. He, J.T. Tang, J. Shen, J.M. Chen, S. Song, *Appl. Surf. Sci.* 364 (2016) 416–427.
- [16] S.Q. Liu, C. Han, Z.R. Tang, Y.J. Xu, *Mater. Horiz.* 3 (2016) 270–282.
- [17] Z. Jin, Q. Wang, W. Zheng, X. Cui, *ACS Appl. Mater. Interfaces* 8 (2016) 5273–5279.
- [18] W. Tu, Y. Zhou, H. Li, P. Li, Z. Zou, *Nanoscale* 7 (2015) 14232–14236.
- [19] N. Zhang, C. Han, Y.J. Xu, J.J. Foley, D.T. Zhang, J. Codrington, S.K. Gray, Y.G. Sun, *Nat. Photonics* 10 (2016) 473–483.
- [20] N. Zhou, L. Polavarapu, N. Gao, Y. Pan, P. Yuan, Q. Wang, Q.H. Xu, *Nanoscale* 5 (2013) 4236–4241.
- [21] D. Kong, J.Z.Y. Tan, F. Yang, J.L. Zeng, X.W. Zhang, *Appl. Surf. Sci.* 277 (2013) 105–110.
- [22] Z. Zhang, Z. Wang, S.-W. Cao, C. Xue, *J. Phys. Chem. C* 117 (2013) 25939–25947.
- [23] K. Kontapakdee, J. Panpranot, P. Praserthdam, *Catal. Commun.* 8 (2007) 2166–2170.
- [24] H.Y. Yin, X.L. Wang, L. Wang, Q.L. Nie, Y. Zhang, W.W. Wu, *Mater. Res. Bull.* 72 (2015) 176–183.
- [25] R. Liu, A. Sen, *J. Am. Chem. Soc.* 134 (2012) 17505–17512.
- [26] K. Khaletskaya, A. Pougin, R. Medishetty, C. Rösler, C. Wiktor, J. Strunk, R.A. Fischer, *Chem. Mater.* 27 (2015) 7248–7257.
- [27] Y.S. Chen, P.V. Kamat, *J. Am. Chem. Soc.* 136 (2014) 6075–6082.
- [28] C. Wang, D. Astruc, *Chem. Soc. Rev.* 43 (2014) 7188–7216.
- [29] B. Mei, A. Pougin, J. Strunk, *J. Catal.* 306 (2013) 184–189.
- [30] J.Q. Jiao, Y.C. Wei, Z. Zhao, W.J. Zhong, J. Liu, J.M. Li, A.J. Duan, G.Y. Jiang, *Catal. Today* 258 (2015) 319–326.
- [31] M. Tahir, B. Tahir, N.A.S. Amin, *Appl. Surf. Sci.* 356 (2015) 1289–1299.
- [32] Y. Bu, S. Lee, *ACS Appl. Mater. Interfaces* 4 (2012) 3923–3931.
- [33] Y.A. Attia, D. Buceta, C. Blanco-Varela, M.B. Mohamed, G. Barone, M.A. Lopez-Quintela, *J. Am. Chem. Soc.* 136 (2014) 1182–1185.
- [34] E. Liu, Y. Hu, H. Li, C. Tang, X. Hu, J. Fan, Y. Chen, J. Bian, *Ceram. Int.* 41 (2015) 1049–1057.
- [35] S. Kamimura, T. Miyazaki, M. Zhang, Y. Li, T. Tsubota, T. Ohno, *Appl. Catal. B: Environ.* 180 (2016) 255–262.
- [36] G.O. Larrazábal, A.J. Martín, S. Mitchell, R. Hauer, J. Pérez-Ramírez, *J. Catal.* 343 (2016) 266–277.
- [37] S.W. Verbruggen, M. Keulemans, M. Filippoussi, D. Flahaut, G. Van Tendeloo, S. Lacombe, J.A. Martens, S. Lenaerts, *Appl. Catal. B: Environ.* 156–157 (2014) 116–121.
- [38] P. Du, J.T. Cameiro, J.A. Moulijn, G. Mul, *Appl. Catal. A* 334 (2008) 119–128.
- [39] P.V.R.K. Ramacharyulu, J. Praveen kumar, G.K. Prasad, A.R. Srivastava, *RSC Adv.* 5 (2015) 1309–1314.
- [41] S.P. Lim, A. Pandikumar, N.M. Huang, H.N. Lim, *RSC Adv.* 4 (2014) 38111–38118.
- [42] B. Choudhury, R. Verma, A. Choudhury, *RSC Adv.* 4 (2014) 29314.
- [43] T. Tanvi, A. Mahajan, R.K. Bedi, S. Kumar, V. Saxena, A. Singh, D.K. Aswal, *RSC Adv.* 6 (2016) 48064–48071.
- [44] K.L. Goeken, V. Subramaniam, R. Gill, *Phys. Chem. Chem. Phys.* 17 (2015) 422–427.
- [45] C.M. Cobley, S.E. Skrabalak, D.J. Campbell, Y. Xia, *Plasmonics* 4 (2009) 171–179.
- [46] L. Sinatra, A.P. LaGrow, W. Peng, A.R. Kirmani, A. Amassian, H. Idriss, O.M. Bakr, *J. Catal.* 322 (2015) 109–117.
- [47] B. Tahir, M. Tahir, N.A.S. Amin, *Appl. Surf. Sci.* 338 (2015) 1–14.
- [48] J. Fang, S.-W. Cao, Z. Wang, M.M. Shahjamali, S.C.J. Loo, J. Barber, C. Xue, *Int. J. Hydrogen Energy* 37 (2012) 17853–17861.